

Communication

Preparation and Corrosion Resistance of Superhydrophobic Coatings on 7005 Aluminum Alloy

Huilan Huang ^{1,2}, Feng Guo ^{3,4}, Xintao Li ^{1,2}, Peng Xia ^{5,*}, Li Yang ¹ and Chuanbo Hu ^{3,6} 

¹ Institute of New Materials, Guangdong Academy of Sciences, Guangzhou 510650, China; huanghuilan@gdinm.com (H.H.); lixitao@gdinm.com (X.L.); yangli@gdinm.com (L.Y.)

² Jiangxi Universal New Materials Lightweight Industrial Technology Research Institute, Shangrao 334000, China

³ Key Laboratory of Water Environment Evolution and Pollution Control in Three Gorges Reservoir, Chongqing Three Gorges University, Chongqing 404100, China; gf_118099@163.com (F.G.); huchuanbo@hkbu.edu.hk (C.H.)

⁴ Material Corrosion and Protection Key Laboratory of Sichuan Province, Zigong 643000, China

⁵ School of Material Science and Engineering, Dongguan University of Technology, Dongguan 523808, China

⁶ Department of Chemistry, Hong Kong Baptist University, Hong Kong 999077, China

* Correspondence: xiapeng@dgu.edu.cn

Abstract: Composite coatings on the surface of a semi-continuous cast 7005 aluminum alloy under different aging treatments (T6, RRA, and FSA) are presented and characterized in this research. SiO₂ combined with stearic acid (STA) modified by KH550 was utilized to achieve multifunctional superhydrophobic coatings. Adhesive tape adhesion, blade scratch, and mechanical wear tests were utilized to assess the durability of the superhydrophobic coatings. The results showed that the prepared coatings exhibited excellent superhydrophobicity, self-cleaning ability, and mechanical properties, especially the T6 temper alloy. This alloy had the largest CA value (156.5°) and the lowest SA value (4.3°). The composite coatings still exhibited excellent superhydrophobicity under mechanical damage. Furthermore, the alloys with STA/SiO₂ displayed marvelous corrosion resistance efficiency. The T6 temper alloy with a protection rate of 73.8% had an approximately one-order-of-magnitude decrement in carriorn current density. The composite coating can be effectively utilized in various industrial fields, thus extending its potential impact.

Keywords: 7005 aluminum alloy; multistage aging treatment; superhydrophobic; sol-gel



Citation: Huang, H.; Guo, F.; Li, X.; Xia, P.; Yang, L.; Hu, C. Preparation and Corrosion Resistance of Superhydrophobic Coatings on 7005 Aluminum Alloy. *Coatings* **2024**, *14*, 499. <https://doi.org/10.3390/coatings14040499>

Academic Editor: Joachim Albrecht

Received: 11 December 2023

Revised: 29 March 2024

Accepted: 9 April 2024

Published: 17 April 2024



Copyright: © 2024 by the authors. Licensee MDPI, Basel, Switzerland. This article is an open access article distributed under the terms and conditions of the Creative Commons Attribution (CC BY) license (<https://creativecommons.org/licenses/by/4.0/>).

1. Introduction

Al-Mg-Zn alloys have been widely used in transportation, construction, packaging, and other fields because of their good mechanical properties, low density, thermal conductivity, and other characteristics [1]. A dense oxide film on the surface of an aluminum alloy has a protective effect, which will fail when exposed to a humid environment for a long time, leading to eventual corrosion [2–4]. Therefore, many experts are dedicated to finding more methods for manufacturing anticorrosive materials, particularly focusing on creating superhydrophobic surfaces on aluminum alloys [5–10]. Moreover, superhydrophobicity has drawn significant attention from the research community due to its potential value in self-cleaning as well as ice and corrosion resistance [11,12].

However, researchers utilize chemicals to produce mechanically strong, self-healing superhydrophobic surfaces, which are harmful to the environment and human health [13–16]. Therefore, researchers have shifted their focus towards developing economical, simple, and environmentally friendly methods for preparing stable superhydrophobic coatings. It is known that producing superhydrophobic coatings requires not only microscopic geometric roughness but also low surface energy to attain surface hydrophobicity [17,18]. SiO₂ and stearic acid are appropriate materials for preparing good superhydrophobic coatings [19–22]. For instance, Li et al. [23] utilized hydroxyapatite (HA)/stearic acid to modify

a magnesium alloy and then acquired a durable superhydrophobic coating with long-term stability. Meanwhile, it is worth noting that aluminum alloys (1060, 2024, 5052, 6061, 7075) with superhydrophobic surfaces have excellent self-cleaning properties and corrosion resistance [24]. It is also known that Al-Mg-Zn alloys with multistage aging treatments have different levels of corrosion resistance, while the T6 temper alloy has the highest strength and the lowest corrosion resistance [25]. Therefore, surface modification may be a cost-effective way to improve the corrosion resistance of the T6 temper aluminum alloy.

In this research, an organic/inorganic hybrid superhydrophobic coating was prepared using coarse-structured SiO_2 , stearic acid with a low surface energy, and silane coupling agent (KH550). This study introduces the preparation of organic/inorganic hybrid superhydrophobic composite coatings with good corrosion resistance on 7005 aluminum alloy by the sol-gel method. The novelty lies in dispersing nanoparticles into a polymer material to create a superhydrophobic nanocomposite coating. Importantly, the manufacturing process does not require complex instruments or special/expensive reagents. This method offers non-fluorinated and environmentally friendly characteristics, making it suitable for corrosion protection across different metal substrates. The purpose of this research was to fabricate a surface with high superhydrophobicity, good mechanical and chemical stability, high corrosion resistance, and excellent self-cleaning ability. The simplicity and low cost of the developed method will enhance its suitability for large-scale production.

2. Experimental Section

2.1. Material and Sample Preparation

In this study, 7005 aluminum alloy (Al-Zn-Mg alloy) plates with sizes of $1 \times 1 \text{ cm}^2$, $2 \times 2 \text{ cm}^2$, and $2 \times 4 \text{ cm}^2$ were used as substrates, and the actual chemical composition of the alloy is listed in Table 1. They were prepared in three different heat treatment conditions, such as a peak-aged condition (T6), retrogression and re-ageing condition (RRA), and four-stage ageing condition (FSA). The samples were repeatedly polished using sandpaper with different particle sizes. And then, the samples were cleaned with acetone and ethanol. After that, they were ultrasonically cleaned with ethanol for 10 m, then rinsed with distilled water and finally dried at room temperature.

Table 1. The actual composition of 7005 aluminum alloy.

Element	Si	Fe	Mn	Mg	Cr	Zn	Ti	Zr	Al
Content%	0.052	0.075	0.31	1.28	0.13	4.98	0.028	0.14	Bal.

SiO_2 nanoparticles with an average particle size of 50 nm were used in the research. Stearic acid ($\text{C}_{18}\text{H}_{36}\text{O}_2$ /STA, analytical grade) and acetone ($\text{C}_3\text{H}_6\text{O}$, analytical grade) were provided by Chron Chemical Co., Ltd., Chengdu, China. Ethanol ($\text{C}_2\text{H}_6\text{O}$, analytical grade) was purchased from Chuandong Chemical Co., Ltd., Chongqing, China. 3-Aminopropyltriethoxysilane (namely silane coupling agent KH550, analytical grade) was supplied by Chenguang Coupling Agent Co., Ltd., Nanjing, China. All the materials were analytically pure without any further purification.

2.2. Superhydrophobic Coating Fabrication

Figure 1 shows a schematic diagram of a preparation procedure of an organic/inorganic hybrid superhydrophobic composite coating (SKS) on a 7005 aluminum alloy substrate. The procedure involved a two-step method. The first step was to acquire the STA- SiO_2 modification solution. Firstly, certain amounts of SiO_2 nanoparticles (1.5 g), ethanol (20 mL), and stearic acid (2 g) were successively added to a beaker. The mixture was weighed, stirred for several hours until completely dissolved in a magnetic mixer, and finally dried. Subsequently, the dried power (1.5 g) was weighed and dissolved in ethanol (20 mL). Then, KH550 (1 g) was added and stirred evenly to obtain a modification solution. The second step was to fabricate the superhydrophobic coating. The polished and cleaned aluminum

alloy substrates were dipped in and out of the modification solution several times. The substrates were dried at room temperature for 30 m and cured at 55 °C for 1 h to yield the composite coating.

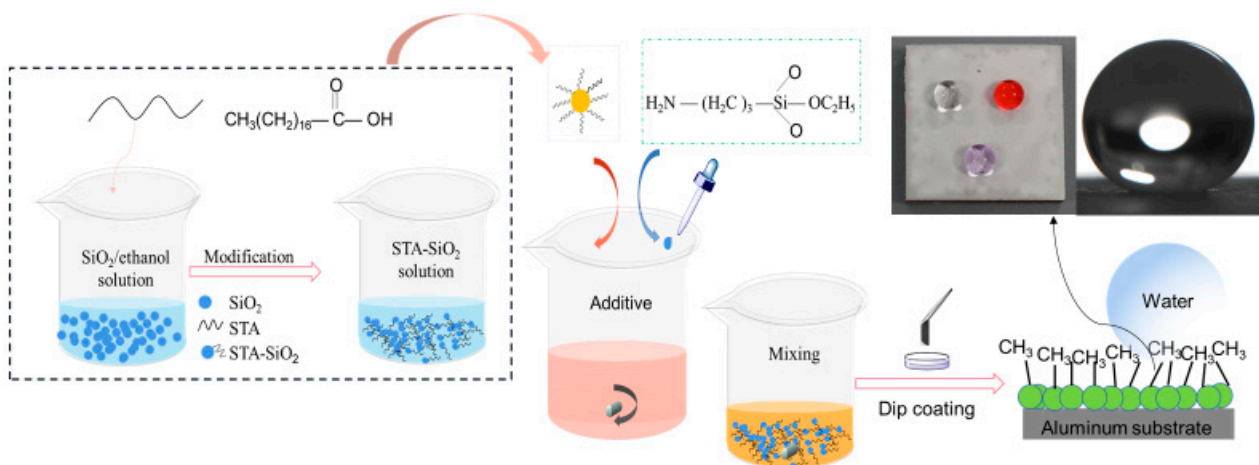


Figure 1. A schematic diagram of the fabrication of superhydrophobic coating on 7005 aluminum alloy.

2.3. Characterization

The surface morphology of the samples was observed in a Zeiss Gemini SEM 300 field-emission scanning electron microscope. X-ray diffraction patterns of SiO_2 and the modified coating were characterized by an X-ray diffractometer (XRD, Rigaku, Tokyo, Japan) at a scanning rate of 4°/min. The surface chemical compositions of the samples before and after modification were investigated by X-ray photoelectron spectroscopy (XPS, thermoKalpha, Shanghai, China) and Fourier-transform infrared spectroscopy (FTIR, Shanghai, China). The contact angle (CA) and sliding angle (SA) of the samples were measured at room temperature using a Dataphysic-OCA20 measuring instrument (SDC-80). For the accuracy of the experiment, the water CA and SA were the average values of five different positions on each sample measured with 3 μL of water droplets. Electrochemical corrosion tests to evaluate the electrochemical performance of the samples were carried out using a Versa Studio electrochemical workstation with a conventional three-electrode cell. The reference electrode was a saturated calomel electrode (SCE), while the platinum electrode and the samples were used as a counting electrode and working electrode, respectively. All the samples were required to be immersed in NaCl solution (3.5 wt. %) for 30 min to stabilize the free corrosion potential before electrochemical testing. Tafel polarization curves were recorded at a constant scanning rate of 1 mV/s in the open potential range of -250 to 250 mV.

3. Results and Discussion

3.1. Surface Characterization

It is well known that a superhydrophobic surface is characterized by both a large static CA ($\geq 150^\circ$) and a small SA ($\leq 10^\circ$) [26]. Figure 2 illustrates the morphology of water droplets and the corresponding CA and SA values on the surfaces of the RRA-, T6-, and FSA-temper samples. The water droplets were dyed with red and purple ink to better display the shape and outline. Notably, the water droplets on the surface of the composite coating appear approximately spherical, and the CA values of the RRA-, T6-, and FSA-temper samples are all greater than 150° , while the corresponding SA values are all less than 5° . The results, as shown in Figure 2b, indicate that the CA and SA values of the T6-temper sample were 156.5° and 4.3° , respectively. Compared to the RAA and FSA-temper samples, the T6-temper sample shows an excellent superhydrophobic performance.

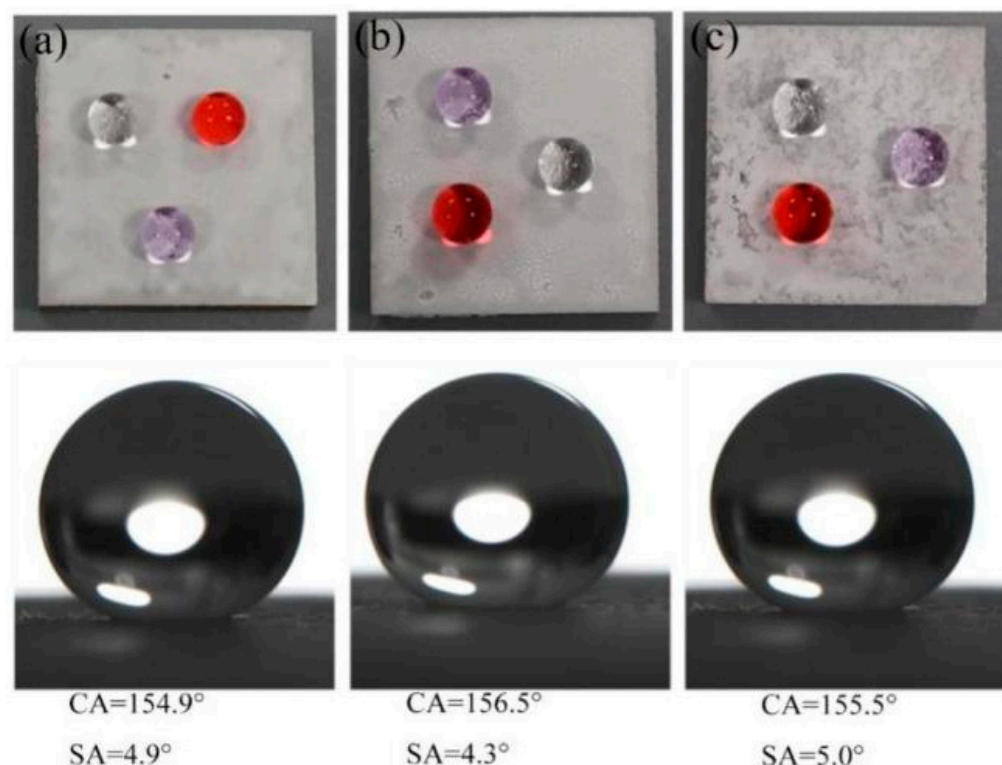


Figure 2. Images of the dyed water droplets on the surface; CA and SA values of (a) RRA-, (b) T6-, and (c) FSA temper samples.

The SEM images of modified SiO_2 powder were obtained to confirm the surface morphology and layered microstructure. Figure 3 shows SEM images of the RRA, T6, and FSA temper samples modified with SiO_2 powders. As shown in Figure 3d–f, it is evident that the coating comprises micro-scale protrusions with spherical microscopic characteristics at the top. These spherical microscopic characteristics are composed of silica colloidal particles. Low-surface-energy materials were filled into these circular holes during the subsequent preparation of the composite coating. The KH550 combined with modified silica nanoparticles formed an island distribution, thereby developing a micro/nanostructure.

As shown in Figure 4a, no significant difference can be observed in the FTIR spectra of the pure SiO_2 and modified SKS powders. The wide and strong peaks near 1058 cm^{-1} represent asymmetric Si–O–Si antisymmetric stretching vibration, while the absorption bands near 790 cm^{-1} and 450 cm^{-1} correspond to symmetric Si–O–Si stretching and bending vibration peaks. These three absorption peaks are typical absorption peaks of pure SiO_2 powders. It can be concluded that the infrared spectrum is consistent with the reported literature [27,28]. However, the absorption peaks near 2920 cm^{-1} and 2850 cm^{-1} of the SKS samples are attributed to CH_3 and CH_2 . It is indicated that the KH550 covalently binds to the surface of SiO_2 nanoparticles, successfully chemically modifying the surface [29]. The increased depth of the absorption peaks is mainly due to the presence of symmetric and asymmetric stretching vibrational peaks of the C–H bond in stearic acid. To elucidate the relationship between surface chemical element composition and superhydrophobic properties, XPS spectra was employed to conduct detailed chemical bond analysis on the surfaces of RRA, T6, and FSA temper sample. The O1s, C1s, and Si2p peaks originating from the substrate are shown in Figure 4b and Table 2, respectively. Compared to unmodified SiO_2 , the O and Si contents of the modified SiO_2 decreased significantly, while the C content increased markedly. This change is due to the higher C content in the silane coupling agent compared to SiO_2 , implying the presence of an organic layer on the silicon carbide surface. Figure 4c,d illustrate the high-resolution region scanning results of the SiO_2 and SKS

powders. In the C1s spectra of the SKS powders, the coating can be fitted into C–C, C–H and Si–C (284.8 eV), and C–O (286.6 eV). Additionally, two peaks with similar areas located at 102.2 eV and 103.6 eV in the Si2p window are considered to be Si–O–Si and nano-silica, respectively. It can be concluded that no new chemical bonds are formed by modification and the surface is covered with a long-chain alkyl, which further indicates that KH550 is grafted on the surface.

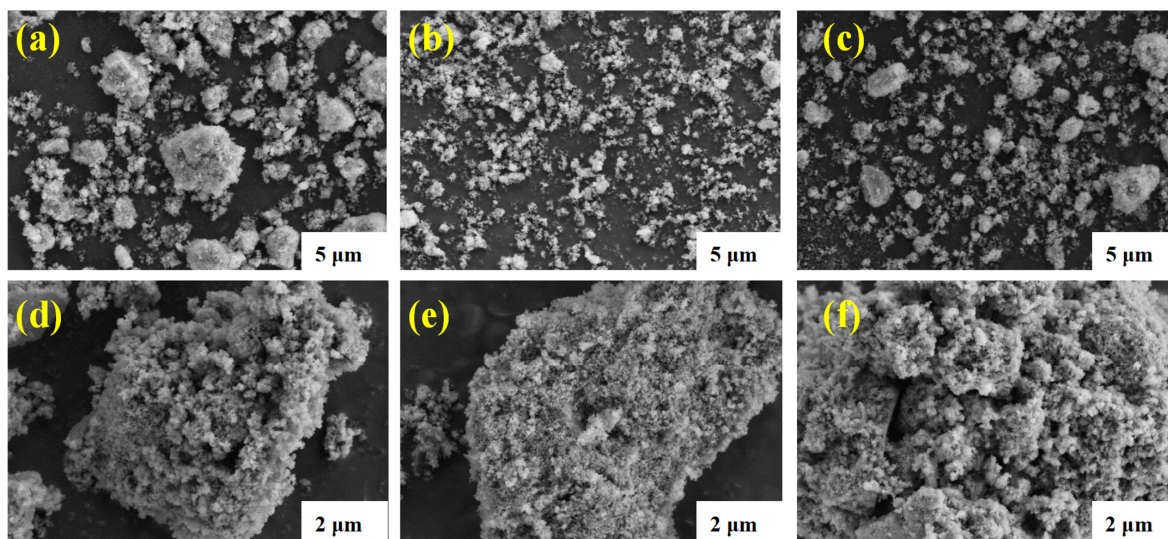


Figure 3. SEM images and corresponding high-magnification SEM images of (a,d) RRA, (b,e) T6, and (c,f) FSA temper samples modified with SiO_2 particles.

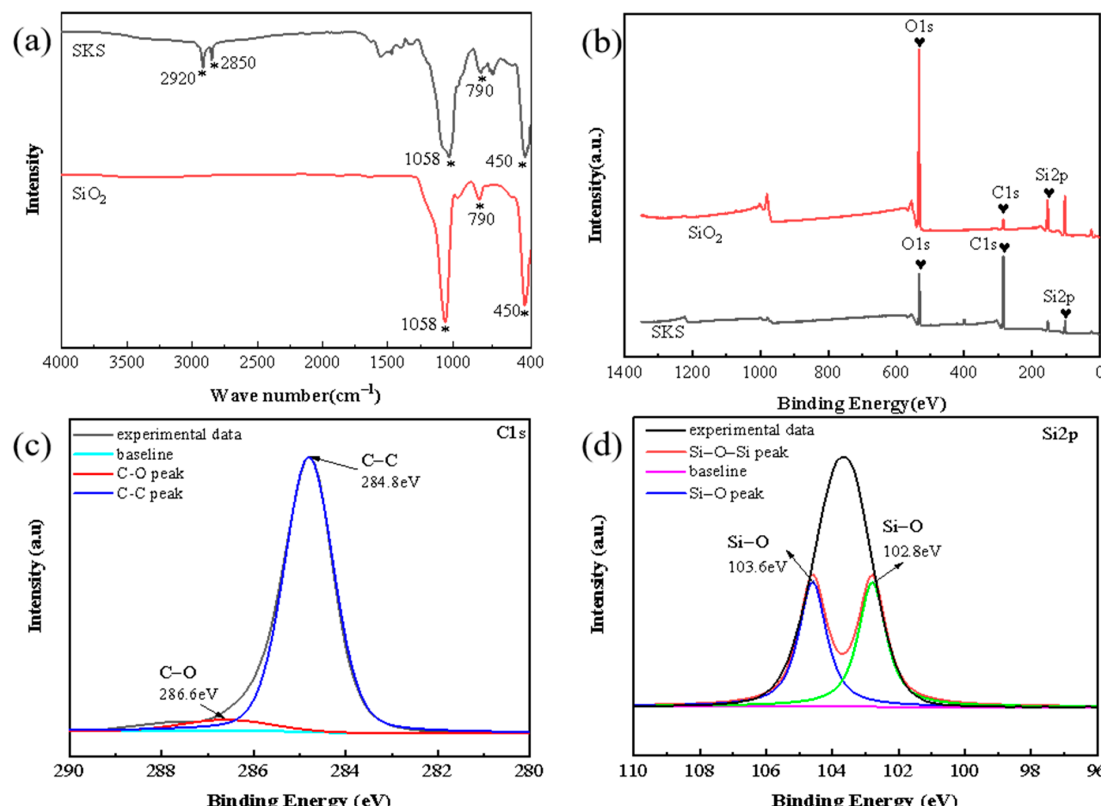
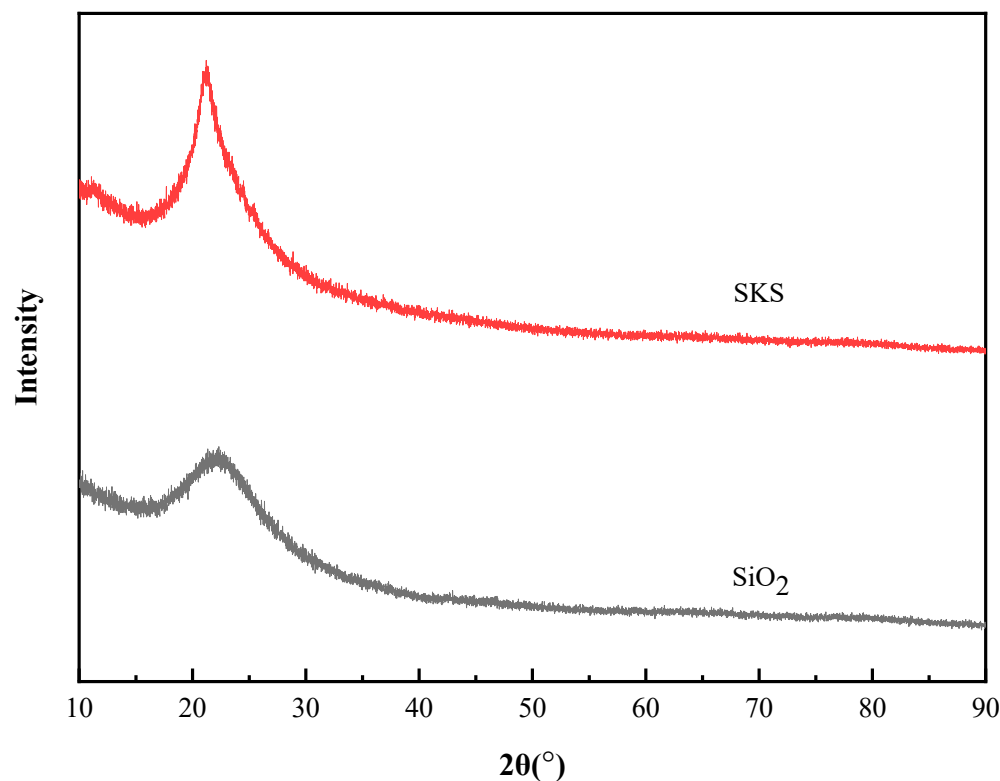


Figure 4. (a) FTIR spectra and (b) XPS survey spectra of SiO_2 and SKS powders; (c) C1s and (d) Si2p bands in high-resolution spectra.

Table 2. XPS survey spectra of the most concentrated elements before and after modification.

Samples	Peak Designation	Band (eV)	Atomic (%)
SiO ₂ powder	C	284.8	7.67
	Si	103.6	62.1
	O	532.8	30.24
SiO ₂ -KH550	C	284.8	57.1
	Si	102.8	13.9
	O	532.2	22.62

Figure 5 depicts the X-ray diffraction (XRD) patterns of the unmodified and modified SiO₂ powders. Upon the analysis of SiO₂ and SKS powders, it was indicated that the wide XRD reflection peak may be attributed to the small size of the prepared particles and the incomplete internal structure. The curves with a high degree of coincidence indicate that the materials are not simply mixed together. With the addition of KH550, SiO₂ still exhibits an amorphous structure, which indicates that the modification does not alter the crystal structure of SiO₂.

**Figure 5.** XRD pattern of the powders before and after modification.

3.2. Surface Functionality

Figure 6 illustrates the self-cleaning characteristics of the RRA-, T6-, and FSA-temper samples. The samples were tilted at 3° and fine sand particles were dispersed randomly on the surface. Water droplets, assisted by gravity, rolled off the surface, removing the sand particles along their trajectory and leaving a clean surface. As shown in Figure 6a–c in the oblique position, it is evident that the fine sand particles on the surfaces could be easily removed as the water droplets rolled off. The self-cleaning states in the horizontal position are shown in Figure 6d for comparison, which indicates that the water droplets could effectively gather the sand particles on the surface of the three coatings. Therefore, we can draw the conclusion that all the three coatings exhibited self-cleaning properties, and the T6 temper sample demonstrated the most effective self-cleaning behavior.

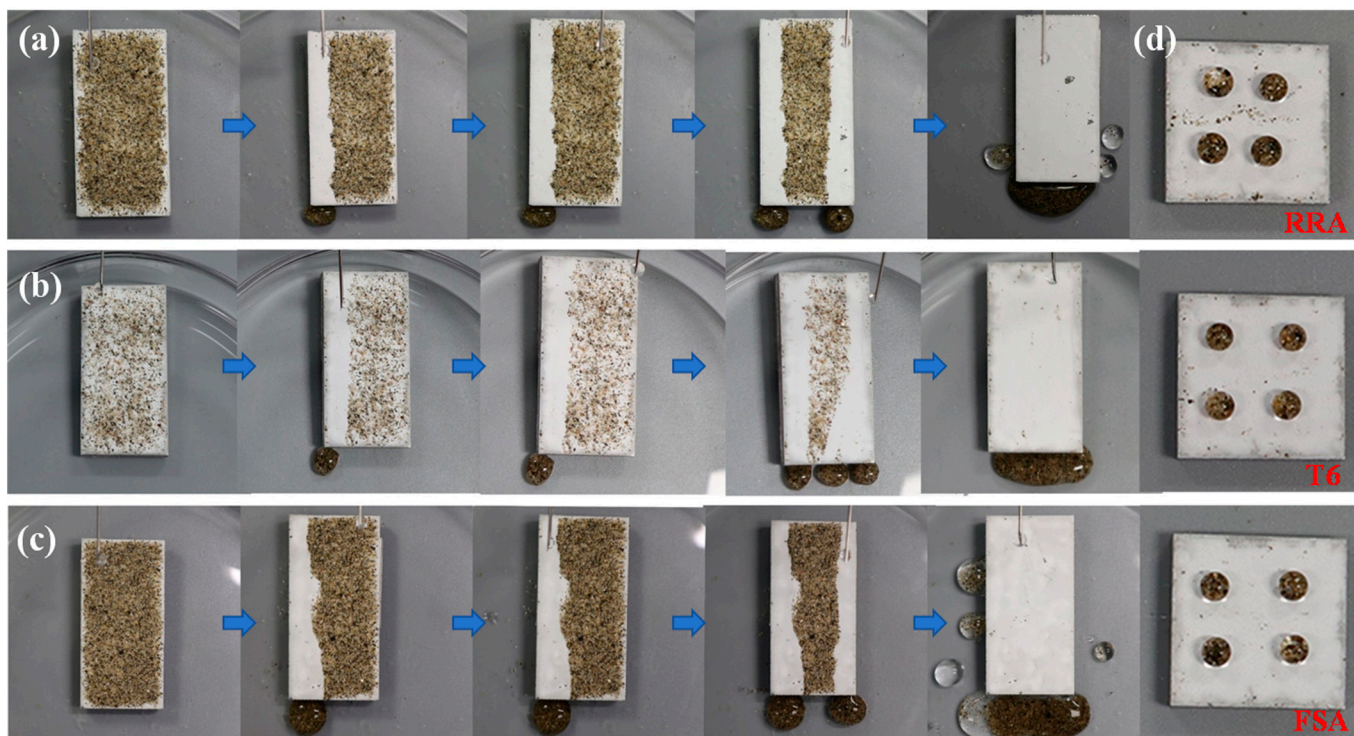


Figure 6. The self-cleaning property procedure of (a) RRA, (b) T6, and (c) FSA samples in oblique position; (d) self-cleaning state in horizontal position of RRA, T6, and FSA samples.

The long-chain molecules on the surface of the modified particles resist agglomeration during the preparation process of coatings. These long-chain molecules are physically entangled or chemically cross-linked with the long-chain molecules of the matrix, which enhances the dispersion and stability of the particle in the coatings. The improved micro- and nano-scale structures trap enough air to form an air cushion, preventing the penetration of the droplets. When pollutants are spread on a low-energy surface, the pollutants are lifted by the air cushion, which can be easily carried away by rolling water droplets.

Adhesive tape and blade scratch peeling tests were applied to evaluate the adhesion of the coatings. Figure 7 provides an illustration of the process for the adhesive tape and blade scratch peeling tests. First, a piece of tape was placed on the surface, and enough pressure was applied on the tape to ensure sufficient contact with the coating. Then, the tape was removed and the water CA of the samples was measured. Figure 7a shows the surface characteristics of a sample before and after adhesive tape peeling. The appearance of the coatings after the adhesive tape peeling was not damaged. Figure 7b shows the detailed process of the blade scratch peeling test and a CA image after the test. The process was performed as follows: First, the surface of the sample was cut and scratched into a rhombic-shape grid with a sharp knife (60 RH). Then, the tape was covered on the surface and pressure was applied to hold it in place. Finally, the tape was removed quickly and the process was repeated 10 times until the desired surface was acquired. It was indicated that the water droplets on the coatings remained non-wetting and the coatings with large CA values (154.6° and 153.9°) maintained high superhydrophobicity. This is attributed to the micro/nanostructure of the aluminum alloy substrate, which enhances the mechanical stability of the coating. Therefore, the coating can be firmly attached to the aluminum alloy substrate.

Mechanical wear is used to further evaluate the mechanical durability of superhydrophobic coatings. The detailed process of the mechanical wear test is as follows: The sample was turned upside down on 1200-grit sand paper, and then the samples were pushed along the straight edge with a weight of 100 g. Figure 8 shows the experimental process of the mechanical wear test on the superhydrophobic surface and corresponding

CA test. The superhydrophobic coating of the sample was pushed 20 cm along the sandpaper, leaving a white mark on the sandpaper. It was observed that water droplets could be placed three-dimensionally on the surface of the sample and still maintained contact after the mechanical wear test, similar to their state before the wear test. The CA and SA values also indicate that the developed coating possessed good superhydrophobicity and wear resistance.

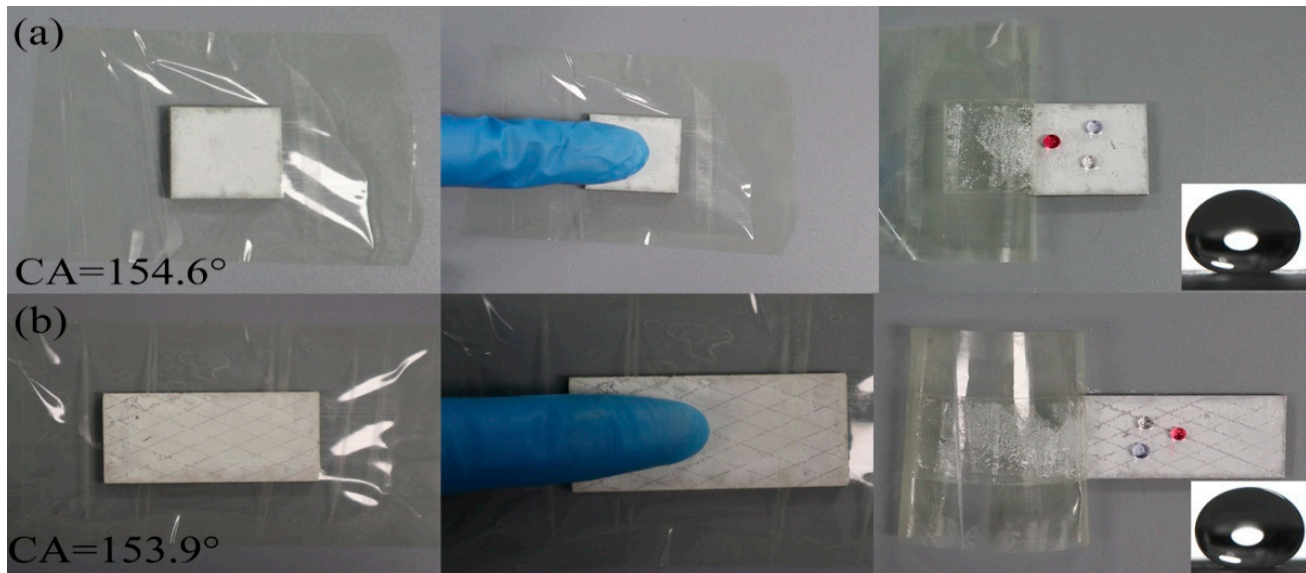


Figure 7. Coating adhesion tests of samples (a) adhesive tape peeling, (b) blade scratch peeling, as well as CA images after the tests.

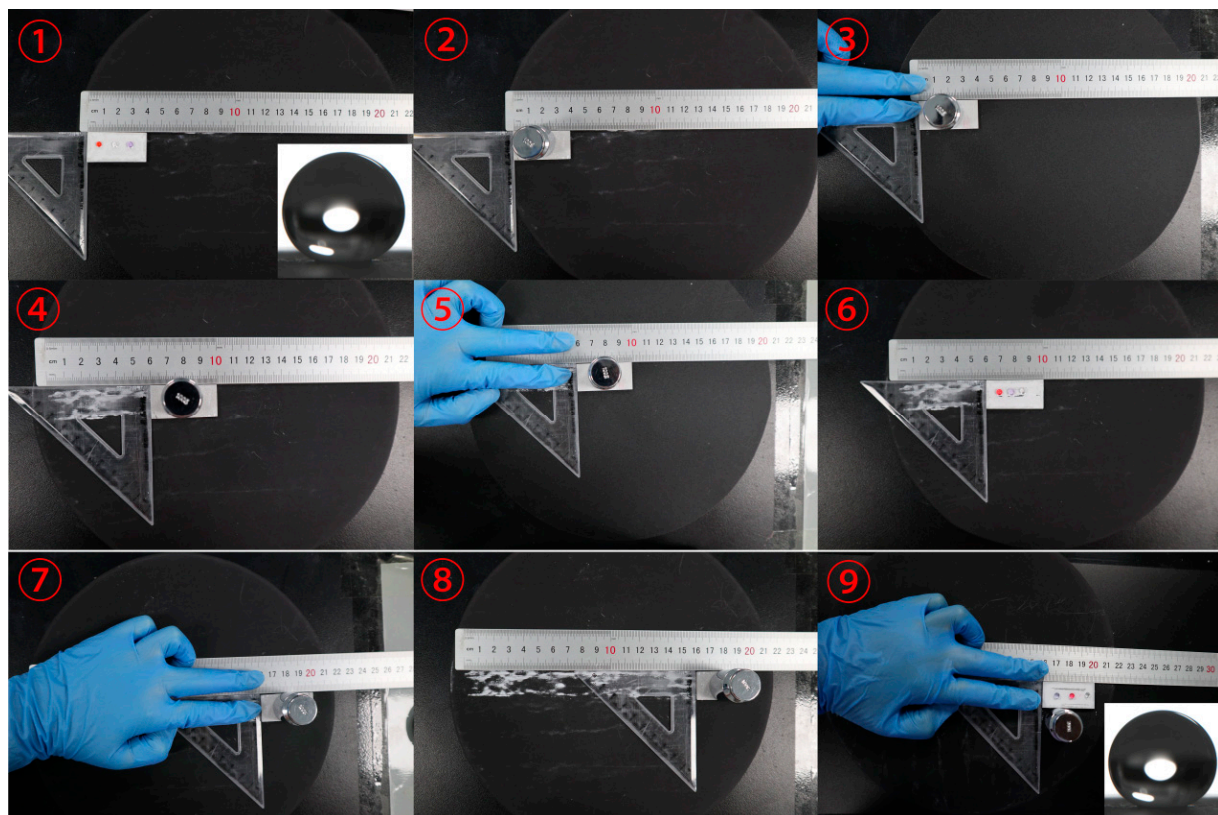


Figure 8. Abrasion resistance test of superhydrophobic coating of RRA temper sample.

Chemical stability is tested to further assess the durability of superhydrophobic coatings. To evaluate the thermal stability of the superhydrophobic coatings in a specific operating environment, samples under different conditions were tested in an oven for 30 min in the temperature range of 25 °C to 200 °C. Figure 9 shows the contact angle of superhydrophobic coatings vs. temperature for the RRA-, T6-, and FSA-tempered samples. It is clear that all the CA values increase with the increase in the temperature, which is attributed to the good thermal stability of the KH550 and SiO₂. Meanwhile, the structure and composition of the surface undergo slight changes, resulting in the maintenance of surface wettability stability. As a result, the superhydrophobic properties of the coating can be sustained within the specified temperature range.

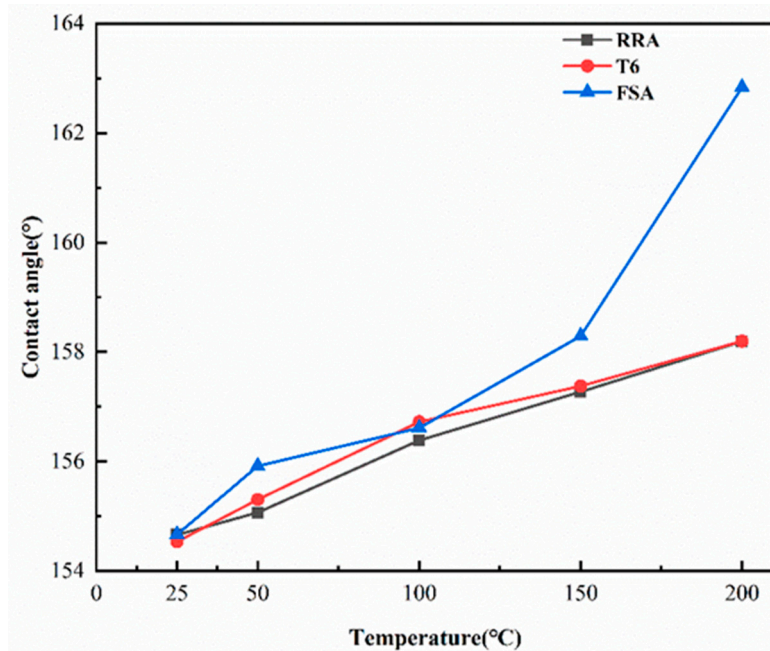


Figure 9. The CA values of coating at different temperatures.

To evaluate the corrosion resistance of the superhydrophobic coatings, electrochemical measurements of the coating were carried out in a corrosive medium. Figure 10 presents the corrosion performance of bare aluminum alloys and superhydrophobic coatings on aluminum alloy substrates under RRA, T6, and FSA conditions in a 3.5 wt. % NaCl solution. The potentiodynamic polarization curves were measured using the three-electrode system, as shown in Figure 10a. It can be clearly seen that the polarization curves of various samples show a similar development trend with the potential increasing, as shown in Figure 10b. However, there were apparent differences in details such as the corrosion potential (E_{corr}) and corrosion current density (I_{corr}) between the bare and coated aluminum samples, indicating different corrosion resistance. Table 3 displays the results of E_{corr} and I_{corr} obtained by the Tafel extrapolation method. Generally, positive E_{corr} and low I_{corr} values represent a weak surface corrosion tendency and slow surface corrosion rate (C_R), respectively. Therefore, alloys with lower I_{corr} and higher E_{corr} values are more likely to be corrosion-resistant coatings. As seen in Table 3, the bare aluminum alloys under RRA, T6, and FSA conditions displayed similar corrosion potential and corrosion current density. Compared to the bare alloys, the surface-treated alloys all showed higher corrosion potential and lower corrosion current density. This is attributed to the presence of a protective layer on the surface-treated alloys. As for the superhydrophobic coatings under RRA, T6, and FSA conditions, the E_{corr} was -0.66 , -0.64 , and -0.89 V, respectively, and the corresponding I_{corr} was 9.57×10^{-5} , 6.05×10^{-5} , and 2.28×10^{-4} A/cm², respectively. The T6-tempered sample coated with STA/SiO₂ exhibited the lowest corrosion current density and almost the highest corrosion potential. It is illustrated that the superhydrophobic

coating can resist strong corrosive media, thus enhancing the corrosion resistance of the coating. The corrosion resistance efficiency (PE) is defined as

$$PE(\%) = \frac{I_{corr} - I_{corr}'}{I_{corr}} \times 100\% \quad (1)$$

where I_{corr} is the self-corrosion current density of a bare aluminum alloy under RRA, T6, and FSA conditions, and I_{corr}' is the self-corrosion current density of the RRA-, T6-, and FSA-tempered samples coated with a dioxide. The PE values of superhydrophobic coatings on the aluminum substrates under RRA, T6, and FSA conditions were calculated as 57.3%, 73.8%, and 16.2%, respectively. The T6-tempered sample coated with STA/SiO₂ displayed the highest corrosion resistance efficiency, which is attributed to the reduction in the contact area with the corrosive medium by the coarse micro- and nano-scale structures of the superhydrophobic coating. Therefore, the superhydrophobic coating can obviously improve the corrosion resistance of the bare aluminum alloy.

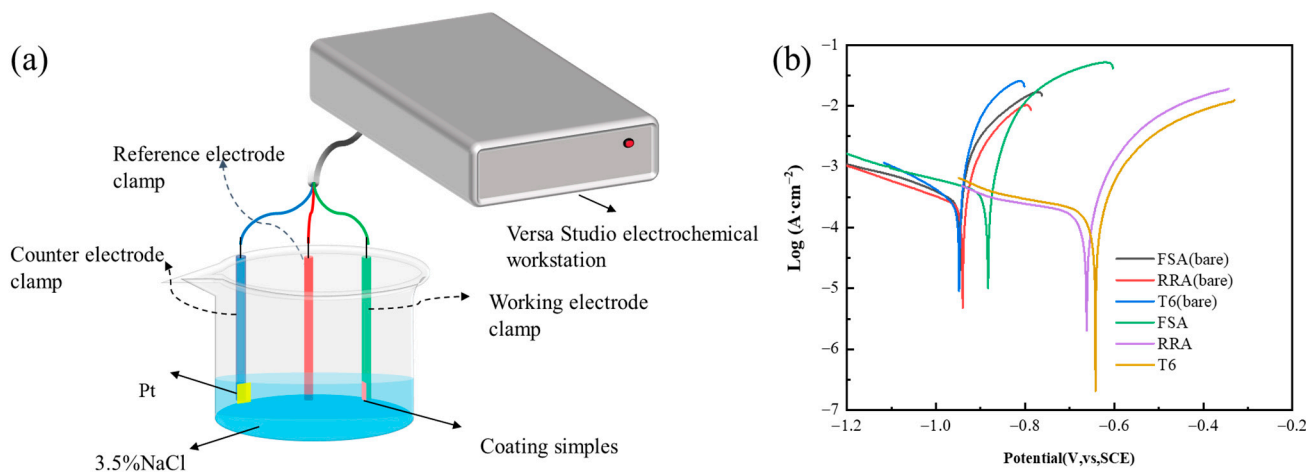


Figure 10. Electrochemical test: (a) electrochemical test mode; (b) Tafel polarization curves of bare alloy and superhydrophobic coating under RRA, T6, and FSA conditions after immersion in 3.5% NaCl aqueous solution for 5 days.

Table 3. The electrochemical corrosion parameters derived by potentiodynamic polarization test.

Samples	E_{corr} (V)	I_{corr} ($A \cdot cm^{-2}$)	PE%
Bare (RRA)	-0.93	2.24×10^{-4}	-
Bare (T6)	-0.95	2.31×10^{-4}	-
Bare (FSA)	-0.95	2.72×10^{-4}	-
RRA	-0.66	9.57×10^{-5}	57.3
T6	-0.64	6.05×10^{-5}	73.8
FSA	-0.89	22.80×10^{-5}	16.2

4. Conclusions

The superhydrophobic and corrosion resistance of a composite coating on 7005 aluminum alloy are described in this research. The alloys coated with STA/SiO₂ all exhibit excellent superhydrophobicity, self-cleaning performance, and corrosion resistance, especially the T6-tempered alloy. The T6-tempered alloy displays the best superhydrophobic properties and the highest corrosion resistance. The composite coatings still exhibit excellent mechanical durability after adhesive tape adhesion, blade scraping, and mechanical wear tests. The multifunctional superhydrophobic coating demonstrates excellent comprehensive performance.

Author Contributions: Conceptualization, C.H.; Methodology, H.H.; Investigation, L.Y. and X.L.; Data curation, F.G.; Writing—original draft, H.H.; Writing—review and editing, P.X.; Funding acquisition, X.L. All authors have read and agreed to the published version of the manuscript.

Funding: This work was financially supported by the Applied Foundation Research of Guangdong Province (Grant No. 2022A1515010001), National Natural Science Foundation of China (Grant No. 52001073), Unveiling and Leading Major Technical Demand Project (Grant No. 2021A005), and National Key Research and Development Program of China (Grant No. 2023YFB3710400).

Institutional Review Board Statement: Not applicable.

Informed Consent Statement: Not applicable.

Data Availability Statement: The data presented in the study are not available due to privacy.

Conflicts of Interest: The authors declare no conflicts of interest.

References

- Calabrese, L.; Khaskhoussi, A.; Patane, S.; Proverbio, E. Assessment of super-hydrophobic textured coatings on AA6082 aluminum alloy. *Coatings* **2019**, *9*, 352. [[CrossRef](#)]
- Zhang, F.; Zhang, C.L.; Song, L.; Zeng, R.C.; Cui, L.Y.; Cui, H.Z. Corrosion resistance of superhydrophobic mg-al layered double hydroxide coatings on aluminum alloys. *Acta Metall. Sin. Engl. Lett.* **2015**, *28*, 1373–1381. [[CrossRef](#)]
- Yin, B.; Fang, L.; Tang, A.Q.; Huang, Q.L.; Hu, J.; Mao, J.H.; Bai, G.; Bai, H. Novel strategy in increasing stability and corrosion resistance for super-hydrophobic coating on aluminum alloy surfaces. *Appl. Surf. Sci.* **2011**, *258*, 580–585. [[CrossRef](#)]
- Barthwal, S.; Lim, S.H. Robust and Chemically Stable Superhydrophobic Aluminum-Alloy Surface with Enhanced Corrosion-Resistance Properties. *Int. J. Precis. Eng. Manuf.-Green Technol.* **2020**, *7*, 481–492. [[CrossRef](#)]
- Liu, Y.; Yin, X.; Zhang, J.; Yu, S.; Han, Z.; Ren, L. A electro-deposition process for fabrication of biomimetic super-hydrophobic surface and its corrosion resistance on magnesium alloy. *Electrochim. Acta* **2014**, *125*, 395–403. [[CrossRef](#)]
- Wu, R.; Jiang, H.; Liu, W.; Deng, J.; Yuan, Z.; Liu, Q.; Chen, H. Bacteriostasis of a super-hydrophobic micro-porous aluminum surface by a facile preparation method. *Adv. Mater. Res.* **2012**, *583*, 346–349. [[CrossRef](#)]
- Fahim, J.; Hadavi, S.M.M.; Ghayour, H.; Tabrizi, S.A.H. Cavitation erosion behavior of super-hydrophobic coatings on Al5083 marine aluminum alloy. *Wear* **2019**, *424–425*, 122–132. [[CrossRef](#)]
- Guo, M.; Ding, B.; Li, X.; Wang, X.; Yu, J.; Wang, M. Amphiphobic nanofibrous silica mats with flexible and high-heat-resistant properties. *J. Phys. Chem. C* **2010**, *114*, 916–921. [[CrossRef](#)]
- Jafari, R.; Farzaneh, M. A simple method to create superhydrophobic aluminium surfaces. *Mater. Sci. Forum.* **2012**, *706–709*, 2874–2879. [[CrossRef](#)]
- Esmaeilirad, A.; Rukosuyev, M.V.; Jun, M.B.G.; van Veggel, F.C.J.M. A cost-effective method to create physically and thermally stable and storable super-hydrophobic aluminum alloy surfaces. *Surf. Coat. Technol.* **2016**, *285*, 227–234. [[CrossRef](#)]
- Huang, W.; Huang, J.; Guo, Z.; Liu, W. Icephobic/anti-icing properties of superhydrophobic surfaces. *Adv. Colloid. Interfac.* **2022**, *304*, 102658. [[CrossRef](#)] [[PubMed](#)]
- Zuo, Z.; Liao, R.; Guo, C.; Yuan, Y.; Zhao, X.; Zhuang, A.; Zhang, Y. Fabrication and anti-icing property of coral-like superhydrophobic aluminum surface. *Appl. Surf. Sci.* **2015**, *331*, 132–139. [[CrossRef](#)]
- Yang, Z.; Liu, X.; Tian, Y. Novel metal-organic super-hydrophobic surface fabricated by nanosecond laser irradiation in solution, Colloids Surfaces A Physicochem. Eng. Asp. **2020**, *587*, 124343. [[CrossRef](#)]
- Hooda, A.; Goyat, M.S.; Pandey, J.K.; Kumar, A.; Gupta, R. A review on fundamentals, constraints and fabrication techniques of superhydrophobic coatings. *Prog. Org. Coat.* **2020**, *142*, 105557. [[CrossRef](#)]
- Zhang, Z.; Zhao, N.; Qi, F.; Zhang, B.; Liao, B.; Ouyang, X. Reinforced superhydrophobic anti-corrosion epoxy resin coating by fluorine–silicon–carbide composites. *Coatings* **2020**, *10*, 1244. [[CrossRef](#)]
- Fu, K.; Lu, C.; Liu, Y.; Zhang, H.; Zhang, B.; Zhang, H.; Zhou, F.; Zhang, Q.; Zhu, B. Mechanically robust, self-healing superhydrophobic anti-icing coatings based on a novel fluorinated polyurethane synthesized by a two-step thiol click reaction. *Chem. Eng. J.* **2021**, *404*, 127110. [[CrossRef](#)]
- Han, B.; Wang, H.; Yuan, S.; Li, Y.; Zhang, X.; Lin, D.; Chen, L.; Zhu, Y. Durable and anti-corrosion superhydrophobic coating with bistratal structure prepared by ambient curing. *Prog. Org. Coat.* **2020**, *149*, 105922. [[CrossRef](#)]
- Quan, Y.Y.; Chen, Z.; Lai, Y.; Huang, Z.S.; Li, H. Recent advances in fabricating durable superhydrophobic surfaces: A review in the aspects of structures and materials. *Mater. Chem. Front.* **2021**, *5*, 1655–1682. [[CrossRef](#)]
- Rasitha, T.P.; Philip, J. Optimal condition for fabricating mechanically durable superhydrophobic titanium surface by rapid breakdown anodization: Self cleaning and bouncing characteristics. *Appl. Surf. Sci.* **2022**, *585*, 152628.
- Liu, X.L.; Gu, Y.C.; Mi, T.F.; Wang, X.M.; Zhang, X. Dip-Coating Approach to Fabricate Durable PDMS/STA/SiO₂ Superhydrophobic Polyester Fabrics. *Coatings* **2021**, *326*, 326. [[CrossRef](#)]
- Luo, Y.; Yao, W.; Fu, W.; Wu, L.; Zhang, D.; Pan, F. Preparing superhydrophobic nanocomposite coating with SiO₂ nanoparticles on magnesium alloy. *Surf. Eng.* **2021**, *37*, 1231–1238. [[CrossRef](#)]

22. Zhao, X.; Li, Y.; Li, B.; Hu, T.; Yang, Y.; Li, L.; Zhang, J. Environmentally benign and durable superhydrophobic coatings based on SiO₂ nanoparticles and silanes. *J. Colloid Interface Sci.* **2019**, *542*, 8–14. [[CrossRef](#)]
23. Li, Q.; Bao, X.; Sun, J.; Cai, S.; Xie, Y.; Liu, Y.; Liu, J.; Xu, G. Fabrication of superhydrophobic composite coating of hydroxyapatite/stearic acid on magnesium alloy and its corrosion resistance, antibacterial adhesion. *J. Mater. Sci.* **2021**, *56*, 5233–5249. [[CrossRef](#)]
24. Liu, W.L.; Wang, S.R.; Wang, G.Q.; Zhang, J.P.; Zhou, C. Investigation on the differences of surface cleaning properties of series of superhydrophobic aluminum alloys. *Colloids Surfaces A Physicochem. Eng. Asp.* **2022**, *651*, 129614. [[CrossRef](#)]
25. Zhang, Z.; Deng, Y.; Ye, L.; Sun, L.; Xiao, T.X. Guo. Effect of multi-stage aging treatments on the precipitation and mechanical properties of Al-Zn-Mg alloys. *Mater. Sci. Eng. A-Struct.* **2020**, *785*, 139394. [[CrossRef](#)]
26. Shirtcliffe, N.J.; McHale, G.; Atherton, S.M.I. Newton. An introduction to superhydrophobicity. *Adv. Colloid Interface* **2010**, *161*, 124–138. [[CrossRef](#)]
27. Hu, Q.; Suzuki, H.; Gao, H.; Araki, H.; Yang, W.; Noda, T. High-frequency FTIR absorption of SiO₂/Si nanowires. *Chem. Phys. Lett.* **2003**, *378*, 299–304. [[CrossRef](#)]
28. Rangelova, N.; Radev, L.; Nenkova, S.; Salvado, I.M.M.; Fernandes, M.H.V.; Herzog, M. Methylcellulose/SiO₂ hybrids: Sol-gel preparation and characterization by XRD, FTIR and AFM. *Cent. Eur. J. Chem.* **2011**, *9*, 112–118. [[CrossRef](#)]
29. Gang, C.; Chen, Q.; Wang, S.; Zhao, J.; Ai, L.; Chen, Q.; Lin, X.; Hu, C. Fabrication of a superhydrophobic SiO₂ coating with anticorrosive protection. *ChemistrySelect* **2023**, *8*, e202300172.

Disclaimer/Publisher’s Note: The statements, opinions and data contained in all publications are solely those of the individual author(s) and contributor(s) and not of MDPI and/or the editor(s). MDPI and/or the editor(s) disclaim responsibility for any injury to people or property resulting from any ideas, methods, instructions or products referred to in the content.